Colloid Polym Sci (2006) 284: 1085–1095
DOI 10.1007/s00396-006-1485-8

ORIGINAL CONTRIBUTION

L. Ceraulo
F. Filizzola
A. Longo
A. Ruggirello
V. Turco Liveri

Physicochemical investigation of the solubilization of ytterbium nitrate in AOT reverse micelles and liquid crystals

Received: 22 September 2005
Accepted: 2 February 2006
Published online: 9 May 2006

L. Ceraulo · F. Filizzola
Dipartimento di Chimica e Tecnologie Farmaceutiche, Università di Palermo,
Via Archirafi 32,
90123 Palermo, Italy

A. Longo
ISMN, Istituto per lo Studio dei Materiali Nanostrutturati CNR,
Via U. La Malfa 156,
90146 Palermo, Italy

A. Ruggirello · V. Turco Liveri (✉)
Dipartimento di Chimica Fisica,
Università di Palermo,
Viale delle Scienze Parco D'Orleans II,
90128 Palermo, Italy
e-mail: turco@unipa.it
Tel.: +39-091-6459844
Fax: +39-091-590015

Abstract A wide investigation of the solubilization of the water-soluble salt $Yb(NO_3)_3$ in sodium bis(2-ethylhexyl) sulfosuccinate (AOT) reverse micelles and AOT liquid crystals has been carried out. After saturation of water/AOT/organic solvent w/o microemulsions with pure $Yb(NO_3)_3$, the $Yb(NO_3)_3$/AOT composites were prepared by complete evaporation under vacuum of the volatile components (water and organic solvent) of the salt-containing microemulsions. It was observed that these composites can be totally dissolved in pure n-heptane or CCl_4, allowing the solubilization of a noticeable amount of $Yb(NO_3)_3$ in quite dry apolar media. By UV–vis–NIR, FT-IR, and ^{1}H NMR spectroscopies, some information on the state of $Yb(NO_3)_3$ within AOT reverse micelles were acquired, whereas by small angle X-ray scattering (SAXS), it has been ascertained that $Yb(NO_3)_3$ is quite homogeneously distributed as very small clusters among the reverse micelles. An analysis of SAXS and wide-angle X-ray scattering spectra of $Yb(NO_3)_3$/AOT composites leads to the hypothesis that, also in these systems, $Yb(NO_3)_3$ is dispersed in the surfactant matrix as very small clusters.

Keywords Solubilization · Confinement effects · Ytterbium nitrate · AOT reverse micelles · Ionic clusters

Introduction

Recently, it has been shown that finite amounts of water-soluble inorganic salts can be confined in the hydrophilic domains of surfactant liquid crystals through the following steps: (1) solubilization of the selected salt in w/o microemulsion and (2) complete evaporation under controlled conditions of volatile components (water and apolar solvent) of the salt-containing microemulsion. It was observed that the maximum amount of salt, which can be entrapped in such systems, depends on the water to surfactant molar ratio and on the nature of the salt, surfactant, and apolar solvent [1–5]. Moreover, by resuspending the salt/surfactant composites in apolar solvent, nanoparticles confined in the core of reverse micelles and dispersed in apolar liquid phase can be also obtained.

Using this methodology, surfactant-stabilized nanoparticles of some water-soluble inorganic salts [$CaCl_2$, Na_2HPO_4, $Cu(NO_3)_2$, Na_2S, $ZnSO_4$, $CoCl_2$, $Co(NO_3)_3$] dispersed in sodium bis(2-ethylhexyl)sulfosuccinate (AOT) liquid crystals and AOT/n-heptane solutions have been prepared [2, 6–8]. The physicochemical characterization of these systems emphasized that salt entrapment in the hydrophilic domains of surfactant liquid crystals is accompanied by an increase of lattice parameters and of the structural disorder, whereas the confinement in reverse micelles leads to a slight increase of the micellar core mean radius while the size polydispersity increases significantly. This indicated that, as a consequence of a delicate equilibrium between unlimited growth and random dispersion among reverse micelles, salts are localized as small nanoparticles in the micellar core of some "lucky" reverse

micelles. Besides, due to their smallness and surfactant adsorption at surface, salt nanoparticles show new and distinct physicochemical properties different from those found in bulk [4, 5].

To improve our knowledge on the potentialities of this novel preparation method of liquid crystals and reverse micelles doped with inorganic salts and to shed some light on the microscopic processes involved in the salt confinement within surfactant-based materials, we undertook an investigation of the solubilization of the water-soluble salt $Yb(NO_3)_3$ in water/AOT/n-heptane and water/AOT/CCl_4 microemulsions. We also investigated some physicochemical properties of the $Yb(NO_3)_3$/AOT/n-heptane, $Yb(NO_3)_3$/AOT/CCl_4, and $Yb(NO_3)_3$/AOT systems. Though convenient because both cation and anion can be monitored easily by UV–vis–NIR spectroscopy, this salt has been chosen because it allows the preparation of nanomaterials finding wide applications both in chemistry and biology [9]. Moreover, lanthanide/surfactant composites are potentially useful to realize systems for smart electrochemical applications, emissive LCDs, and magnetooptical devices [10]. On the other hand, AOT is an anionic surfactant possessing two branched alkyl chains, whose liquid crystals and reverse micelles were chosen as solubilizing media since their structural and dynamical properties have been widely investigated [3, 11–13].

Experimental part

Materials

Sodium bis(2-ethylhexyl)sulfosuccinate (AOT, Sigma 99%) was stored in a desiccator and used after at least 1 week. n-Heptane (Aldrich 99%, spectrophotometric grade), carbon tetrachloride (Sigma, 99.97%), ytterbium nitrate pentahydrate (Sigma, ACS reagent) were used as received. Bidistilled water was used in all experiments.

Methods

Preparation of w/o microemulsions

Water/AOT/n-heptane and water/AOT/CCl_4 w/o microemulsions were obtained at various water-to-AOT molar ratios (R_W, R_W=[H_2O]/[AOT]) by adding the appropriate amount of water to the AOT/apolar solvent solution at a fixed AOT concentration. (AOT/n-heptane, [AOT]= 0.066 M; AOT/CCl_4, [AOT]=0.16 M).

Salt-containing w/o microemulsions, at various salt-to-AOT molar ratio (R_S, R_S=[$Yb(NO_3)_3$]/[AOT]), were prepared by adding the appropriate amount of w/o microemulsion to a weighted quantity of salt. An ultrasonic bath was employed to speed up the salt solubilization. At each R_W value, the solubility of $Yb(NO_3)_3$ was determined by visual inspection of samples prepared at various R_S values and kept at constant temperature (25 °C).

Preparation of composites

Evaporation of salt-containing w/o microemulsions was performed using a desiccator connected to a diaphragm vacuum pump (MZ2C, Vacuubrand). To avoid effects due to the evaporation time, the same experimental conditions have been employed for each sample, i.e., initial amount of sample (10 g), shape and volume of sample container (50-cm^3 bottle), and temperature (22±2 °C). In these conditions, it was observed that complete evaporation of the volatile components takes about 1 h. However, all salt–surfactant composites were successively kept under vacuum at least for 2 h.

Preparation of resuspended composites

Full dispersion of the salt/surfactant composites was achieved by adding the appropriate amount of pure n-heptane or CCl_4 to restore the initial AOT concentration. The stability of resuspended composites was checked for a long time (several months); no significant change of the samples was observed. It is worth noting that, even if water is practically absent in the resuspended composites, a considerable amount of salts can be steadily dispersed in an apolar medium.

Apparatus

UV–vis–NIR spectra were recorded in the wavelength range 200–3300 nm with a Perkin Elmer (Lambda-900) spectrometer using Suprasil quartz cells with 1-cm optical path length.

The FT-IR spectra were acquired with a Spectrum BX (Perkin Elmer) spectrometer, using a cell equipped with CaF_2 windows. For all measurements, 100 scans in the 900- to 4,000-cm^{-1} wave number range were carried out. All spectra were recorded with a spectral resolution of 0.5 cm^{-1}.

The ^1H NMR spectra were recorded with a Bruker AC 250 spectrometer operating at a frequency of 250 MHz and using $DMSO_{D6}$ as an external standard.

The small-angle X-ray scattering (SAXS) patterns have been recorded by a laboratory instrumentation consisting of a Philips PW 1830 X-ray generator, providing Cu Kα, Ni-filtered (λ=1.5418 Å) radiation with a Kratky small-angle camera in the "finite slit height" geometry, equipped with step scanning motor and scintillation counter. Each scattering spectrum was subtracted by the cell + solvent contribution. Data were analyzed by the CERN minimization program called MINUITS. Since the SAXS study of

salt-containing reverse micelles in CCl_4 is prevented by a very low micelle/solvent contrast leading to featureless patterns, samples were prepared using n-heptane as the solvent. Taking into account that this substitution involves only minor changes in the structural and dynamical properties of reverse micelles, this choice can be considered a reasonable compromise between the need for further information and the attainable data [14].

X-ray powder diffraction spectra were performed by a Philips diffractometer (PW1050/39 X Change) equipped with a copper anode (Cu Kα, 1.5418 Å).

Solubility measurements and UV–vis–NIR, FT-IR, ^{1}H NMR, SAXS, and wide-angle X-ray scattering (WAXS) spectra of all the samples were performed at 25 °C.

Results and discussion

Solubility

To find the experimental conditions allowing the confinement of the maximum amount of $Yb(NO_3)_3$ in water/AOT/n-heptane and in water/AOT/CCl_4 w/o microemulsions, some preliminary solubility measurements were carried out. These values, expressed as the maximum salt-to-AOT molar ratio ($R_{S,max}$), are shown as a function of the water-to-AOT molar ratio (R_W) in Fig. 1.

The bell-shaped R_W dependence of the solubility is typical of all the salts investigated up to now. It can be rationalized in terms of two opposite factors: the saturation of the water pool, predominant at low R_W, determining an increase of $R_{S,max}$, and the salt effect on the water solubility in w/o microemulsions, predominant at high R_W, causing a decrease of the water solubility and, consequently, of $R_{S,max}$ [6, 15, 16]. According to this explanation, the lower $R_{S,max}$ values observed in water/AOT/CCl_4 w/o microemulsions can be attributed to the lower water solubility in AOT/CCl_4 with respect to that in AOT/n-heptane solutions [17].

UV–vis–NIR spectra

A typical UV–vis–NIR spectrum of $Yb(NO_3)_3$-containing water/AOT/CCl_4 microemulsion ([AOT]=0.16 M, R_W=2.7, R_S=0.05) in the 250- to 1,600-nm wavelength range is shown in Fig. 2. For comparison, the spectrum of AOT/CCl_4 solution at the same AOT concentration is also reported.

It should be noted the band occurring at about 300 nm due to the symmetry-forbidden $n \rightarrow \pi*$ transition of the nitrate anion [18, 19], that at about 974 nm due to the magnetically allowed transition from the $^2F_{7/2}$ to the $^2F_{5/2}$ state of the ytterbium (III) ion [9] and that at about 1,430 nm due to the first overtone of the water OH stretching mode [20]. The intensity of this last band was employed to check the amount of water in all the investigated samples.

The wavelength (λ_{max}) and the molar extinction coefficient (ε_{max}) at the band maximum of both nitrate and Yb (III) ions of all the investigated salt-containing w/o microemulsions are collected in Table 1.

It can be noted that, by decreasing the water content, an ever-increasing deviation of λ_{max} and ε_{max} of the nitrate and Yb(III) ions from those in bulk water (301 and 972 nm, respectively) is observed [9, 18, 19]. This finding suggests that at lower R_W some deviations occur, while at sufficiently high R_W, the coordination shell of both ions confined in water-containing AOT reverse micelles is similar to that in dilute aqueous solutions. Concerning the Yb(III) ion, the observed deviations of λ_{max} and ε_{max} can be reasonably attributed to effects due to a change in the nature of the ligands, i.e., water ligands are more or less extensively substituted by AOT head groups and nitrate ions. On the other hand, the observed spectral deviations of the nitrate ion at low R_W values suggest that, in the highly concentrated and restricted environment of the micellar core, the NO_3^- ion is engaged in ion association with sodium and ytterbium ions. In fact, such interaction

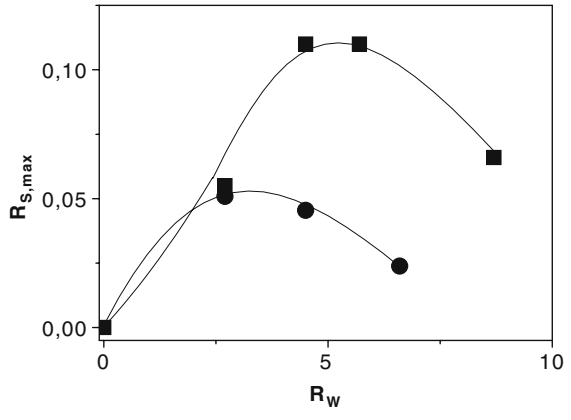

Fig. 1 Solubility ($R_{S,max}$) of ytterbium nitrate in water/AOT/n-heptane (■) and water/AOT/CCl_4 (●) microemulsions as a function of R_W

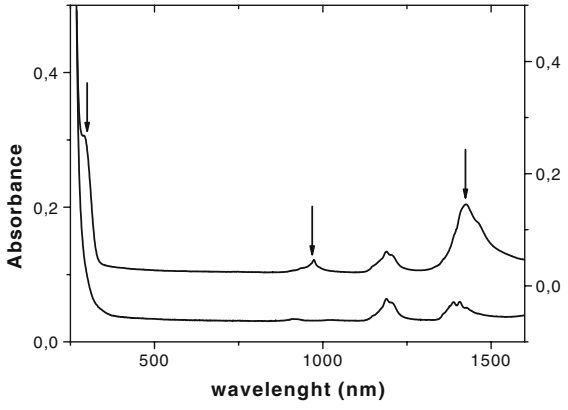

Fig. 2 UV–vis–NIR spectra of $Yb(NO_3)_3$ containing water/AOT/CCl_4 ([AOT]=0.16 M, R_W=2.7, R_S=0.05, *upper spectrum*) and AOT/CCl_4 ([AOT]=0.16 M, *lower spectrum*) systems

Table 1 Wavelength (λ_{max}) and molar extinction coefficient (ε_{max}) at the band maximum of both nitrate and Yb(III) in $Yb(NO)_3$,water/AOT/apolar solvent w/o microemulsions and pure water

R_S	R_W	$\lambda_{max,NO3}$ (nm)	$\varepsilon_{max,NO3}$ ($M^{-1}cm^{-1}$)	$\lambda_{max,Yb}$ (nm)	$\varepsilon_{max,Yb}$ ($M^{-1}cm^{-1}$)
$Yb(NO)_3$,water/AOT/CCl_4 [AOT]=0.16 M					
0.05	2.7	296	7.6	974	2.52
0.04	4.7	298	7.5	974	2.45
0.02	6.6	299	7.3	973	2.31
$Yb(NO)_3$,water/AOT/n-heptane [AOT]=0.066 M					
0.05	2.7	296	7.5	974	2.49
0.11	5.7	298	7.3	974	2.22
0.06	8.7	300	7.2	973	2.17
$Yb(NO)_3$,water [$Yb(NO)_3$]=0.090 M					
		301	7.1	972	1.94

stabilizes the nitrate ion ground state, leading to a hypsochromic shift [18]. It is worth noting that no significant change in the spectral behavior of both nitrate and Yb(III) ions confined in reverse micelles is determined by a variation of the solvent nature, suggesting that they are mainly located in the hydrophilic core of reverse micelles.

A representative UV–vis–NIR spectrum of the $Yb(NO_3)_3$/AOT system, resuspended in CCl_4 ([AOT]=0.16 M, R_W=0.2, R_S=0.05), is compared to that of $Yb(NO_3)_3$-containing water/AOT/CCl_4 microemulsion ([AOT]=0.16 M, R_W=2.7, R_S=0.05) in Fig. 3.

The marked reduction of the water band at about 1,430 nm suggests that water is practically absent in the resuspended samples (the estimated R_W value is 0.2), while the band of both nitrate and Yb(III) appears to be shifted and enhanced with respect to that of the corresponding salt-containing microemulsion. The wavelength (λ_{max}) and the molar extinction coefficient (ε_{max}) at the band maximum of both nitrate and Yb(III) ions of all the investigated resuspended composites are collected in Table 2.

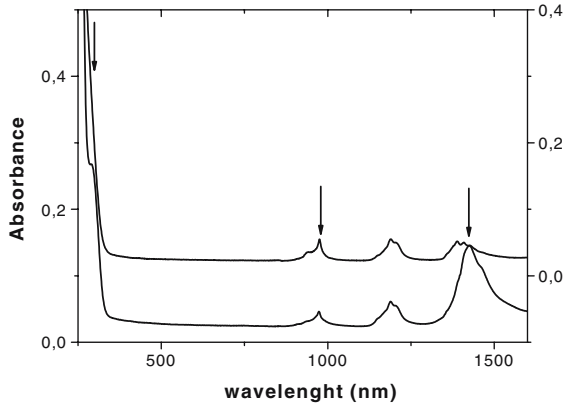

Fig. 3 UV–vis–NIR spectra of $Yb(NO_3)_3$ containing AOT/CCl_4 ([AOT]=0.16 M, R_W=0.2, R_S=0.05, *upper spectrum*) and $Yb(NO_3)_3$ containing water/AOT/CCl_4 ([AOT]=0.16 M, R_W=2.7, R_S=0.05, *lower spectrum*) systems

A perusal of Table 2 leads to the conclusion that λ_{max} and ε_{max} values of both nitrate and Yb(III) ions show the greatest deviations from the corresponding values in water displaying some dependence on the R_S value. It must be stressed that these experimental values reflect the peculiar state of very small clusters composed by ytterbium, sodium, and nitrate ions surrounded by the negative surfactant head groups and confined in the almost dry core of AOT reverse micelles. For this reason, they are of interest and could be used as test standard for theoretical calculations concerning these quite exotic systems.

FT-IR spectra

A typical FT-IR spectrum of $Yb(NO_3)_3$-containing water/AOT/CCl_4 microemulsion ([AOT]=0.16 M, R_W=2.7, R_S=0.05) in the 900- to 4,000-cm^{-1} wavelength range is shown in Fig. 4. For comparison, the spectrum of water/AOT/CCl_4 solution at the same water and AOT concentrations is also reported.

It must be noted that the presence of $Yb(NO_3)_3$ in the micellar core involves some changes in the water OH stretching band (3,000–3,800 cm^{-1}) and in the SO_3^- (~1,050 cm^{-1}) stretching of AOT, as well as the appearance of a new band occurring at 1,250–1,550 cm^{-1} due to the nitrate ion stretching. The observed changes indicate that, as expected, the ytterbium nitrate salt interacts with the AOT head group and water, i.e., the constituents of the hydrophilic core of reverse micelles.

Starting from the water OH stretching band, it must be stressed that this band is a sensitive probe of water state within reverse micelles [21, 22]. This is because a change of the relative populations of differently H-bonded water molecules is revealed by a change in the OH band position, shape, and width. The marked variations induced in the water structure when it is encapsulated within reverse micelles, as well as the effect of the $Yb(NO_3)_3$ presence, are emphasized in Fig. 5, where the water OH band in Yb

Table 2 Wavelength (λ_{max}) and molar extinction coefficient (ε_{max}) at the band maximum of both nitrate and Yb(III) in $Yb(NO_3)_3$/AOT resuspended composites

R_S	R_W	$\lambda_{max,NO3}$ (nm)	$\varepsilon_{max,NO3}$ ($M^{-1}cm^{-1}$)	$\lambda_{max,Yb}$ (nm)	$\varepsilon_{max,Yb}$ ($M^{-1}cm^{-1}$)
$Yb(NO_3)_3$/AOT/CCl_4 [AOT]=0.16 M					
0.05	0.2	277	8.7	975	3.33
0.06	0.2	277	9.3	975	3.54
0.11	0.2	276	10.3	975	3.56
$Yb(NO_3)_3$/AOT/n-heptane [AOT]=0.066 M					
0.05	0.2	278	9.9	976	3.35
0.06	0.2	278	9.9	976	3.49
0.11	0.2	276	10.7	976	3.68

$(NO_3)_3$-containing water/AOT/CCl_4 microemulsions at various R_W and R_S is compared with that of pure water.

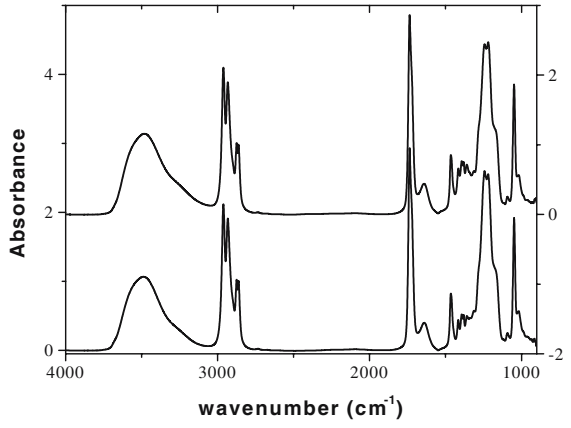

Fig. 4 Infrared spectra of $Yb(NO_3)_3$ containing water/AOT/CCl_4 ([AOT]=0.16 M, R_W=2.7, R_S=0.05, *upper spectrum*) and water/AOT/CCl_4 ([AOT]=0.16 M, R_W=2.7, *lower spectrum*) systems

It can be noted that the OH band of confined water is less broad and centered at higher frequencies, suggesting that it is characterized by a more restricted translational and rotational dynamics and a weaker H-bonding than bulk water [23]. Moreover, by increasing R_W, the OH band trends to that of pure water. This means that further addition of water leads to the formation of a distinct aqueous micellar core, which becomes progressively more bulk-like as a consequence of an increase of its size, while the first water molecules are mainly located as interfacial water bonded to the surfactant head groups SO_3^- and the positive sodium counterions. On the other hand, in the presence of the ytterbium nitrate salt, the contribution of the lower frequency components to the OH band increases. This effect is more evident at lower R_W and/or higher R_S values, and it emphasizes that some water molecules are preferentially engaged in the coordination shell of the Yb^{3+} ions.

Concerning the band (1,250–1,550 cm^{-1}) due to the antisymmetric stretching of nitrate ions, it must be pointed out that it is sensitive to the nature of the surrounding

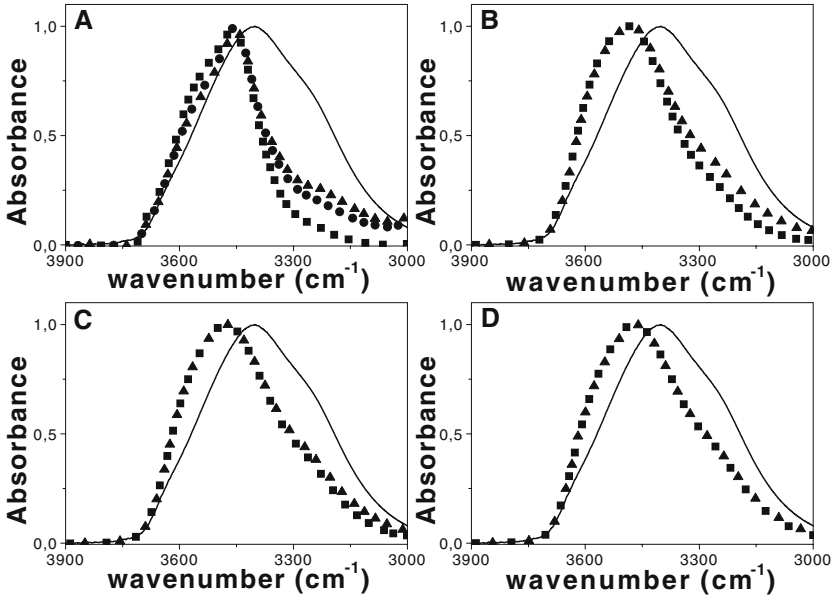

Fig. 5 OH stretching bands of pure water (*continuous line*) and of water in $Yb(NO_3)_3$-containing water/AOT/CCl_4 systems. **a** R_W=0.2 and R_S=0 (■), R_S=0.05 (●) and R_S=0.11 (▲); **b** R_W=2.7, R_S=0 (■) and R_S=0.05 (▲); **c** R_W=4.7, R_S=0 (■) and R_S=0.04 (▲); **d** R_W=6.6, R_S=0 (■) and R_S=0.02 (▲)

species and, in the case of complex formation, to their binding orientation [24]. In particular, formation of solvent-separated ion pairs or uncoordinated nitrate ions are characterized by a broad band occurring in the range 1,345–1,400 cm^{-1} [25, 26]. Whereas, in the case of complex formation with rare earth, a typical monodentate nitrate band shows two peaks at about 1,320 and 1,450 cm^{-1}, while a typical bidentate nitrate band shows one peak at about 1,300 and 1,500 cm^{-1} [24]. The comparison of the antisymmetric stretching band of nitrate ions in $Yb(NO_3)_3$, water/AOT/CCl_4 systems at various R_W and R_S values is shown in Fig. 6.

It can be noted that at R_W=0.2 two peaks at 1,285 and 1,520 cm^{-1} are present, whose relative intensities increase with R_S while that of the band envelope occurring in the range 1,300–1,450 cm^{-1} decreases. According to the literature, this indicates that at R_W=0.2, the nitrate ion is engaged in complex formation with Yb^{3+} as monodentate and bidentate ligand, and that the bidentate fraction increases with R_S. On the other hand, at $R_W \geq 2.7$, the peaks at 1,285 and 1,520 cm^{-1} are absent, while a broad band in the range 1,345–1,400 cm^{-1} occurs. This means that the NO_3^- behaves like solvated free ion and/or as solvent-separated ion pair in such conditions.

Appreciable intensity and position changes due to water and/or ytterbium salt addition are shown by the band centered at about 1,050 cm^{-1} and assigned to the SO_3^- stretching (see Fig. 7).

In particular, by increasing R_W, the band shows a shift toward lower frequencies while its intensity is enhanced. This effect has been previously described and has been attributed to the progressive hydration of the surfactant head group [23]. On the other hand, especially at R_W=0.2, the addition of the ytterbium nitrate in the micellar core shifts the frequency at the band maximum (f^*) toward higher values, suggesting that the SO_3^- group in these conditions is engaged in the first coordination shell of the ytterbium ion (see Fig. 8). The modest or absent shift observed at R_W>0.2 indicates that water competes effectively with the surfactant head group as ligand of the ytterbium ion.

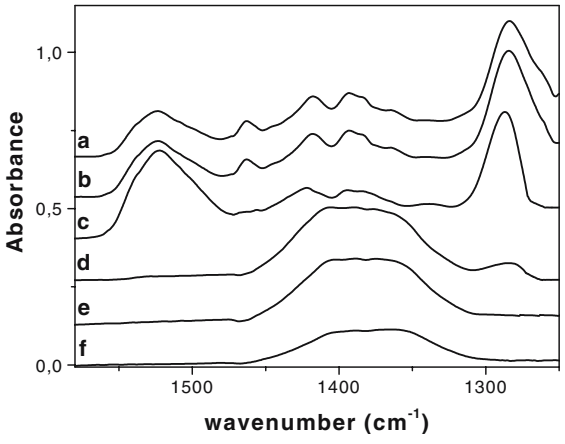

Fig. 6 Antisymmetric stretching band of nitrate ion in ytterbium salt, water/AOT/CCl_4 systems at various R_W and R_S values. **a** R_W=0.2, R_S=0.05; **b** R_W=0.2, R_S=0.06; **c** R_W=0.2, R_S=0.11; **d** R_W=2.7, R_S=0.05; **e** R_W=4.7, R_S=0.04; **f** R_W=6.6, R_S=0.02

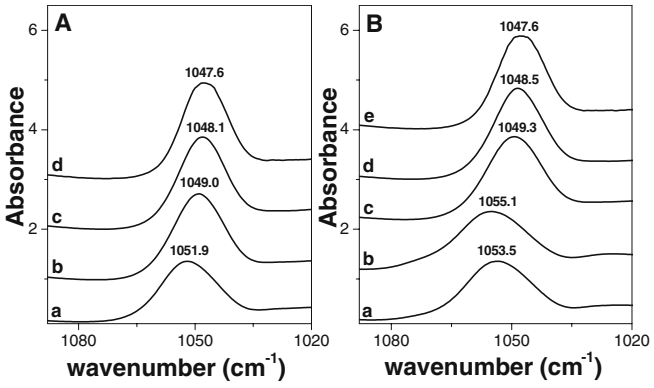

Fig. 7 SO_3^- stretching band of $Yb(NO_3)_3$-containing water/AOT/CCl_4 systems at various R_W and R_S values. **a** R_W=0.2 *a*, R_W=2.7 *b*, R_W=4.7 *c*, R_W=6.6 *d*. **b** R_W=0.2 and R_S=0.05 *a*, R_W=0.2 and R_S=0.11 *b*, R_W=2.7 and R_S=0.05 *c*, R_W=4.7 and R_S=0.04 *d*, R_W=6.6 and R_S=0.02 *e*

^{1}H-NMR spectra

Some representative ^{1}H-NMR spectra of $Yb(NO_3)_3$, water/AOT/CCl_4 systems at various R_W and R_S values are shown in Fig. 9.

It is worth to note that all the spectra were normalized to the same intensity of the peak occurring at 3.33 ppm due to the trace of water present in the external standard. Peak assignment to water and AOT protons was made according to the literature [27, 28], while the chemical shift values are collected in Table 3.

The main feature of these spectra is that, by increasing R_S, water proton peaks vary upfield, whereas those of AOT

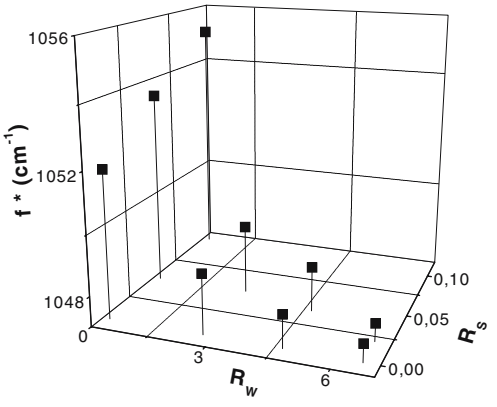

Fig. 8 Frequency (f^*) at the SO_3^- stretching band maximum as a function of R_W and R_S

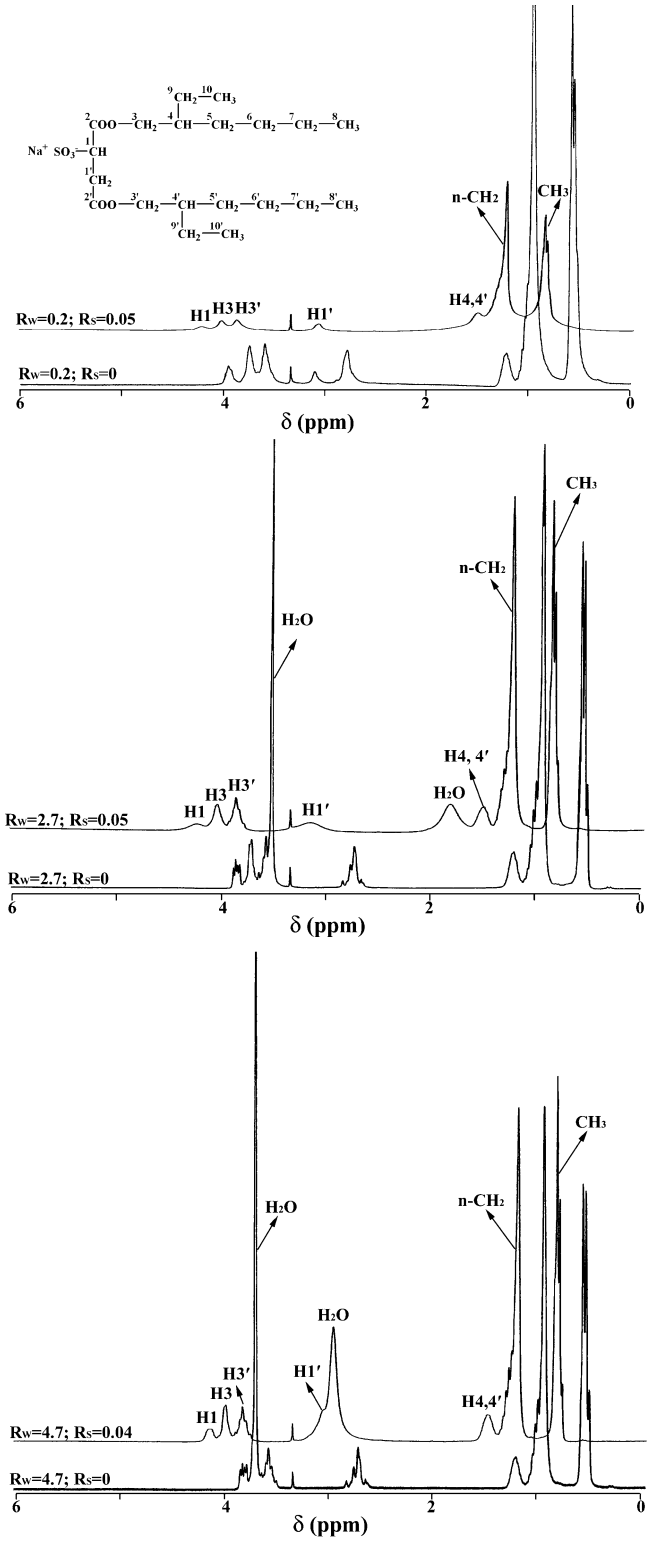

Fig. 9 Effect of water and $Yb(NO_3)_3$ additions on ^{1}H-NMR spectrum of AOT/CCl_4 solution

are shifted to lower fields. A progressive broadening of all the peaks can also be noted [29].

The behavior of the AOT and water protons as a function of R_W, similar to that reported in the literature [30–32], can be similarly attributed to the progressive surfactant head group solvation and change of the water populations confined in the micellar core.

On the other hand, as shown in Fig. 10, the chemical shift of water protons at fixed R_W decreases linearly with R_S and the slope becomes more negative at lower water content. The observed trends suggest that, as a consequence of water binding to the ytterbium ion, the local magnetic field around water protons decreases shifting the peaks to higher fields.

It is important to note that this overwhelming effect is due to the paramagnetism of ytterbium ions. Besides, the more negative slope observed at lower water content can be rationalized, considering that the averaging of the chemical shift on all the water protons involves more marked changes at lower R_W values in the typical time scale of the NMR probe.

The behavior of AOT protons as a function of R_S at various R_W is shown in Fig. 11. The observed linear trends can be attributed to the relevant paramagnetic property of ytterbium ions leading to an enhancement of the local field and, consequently, to a downfield shift of the proton signals.

Considering the slopes (*s*, see Table 3) of these trends, it can be noted that the *s* values of H1′ and H1 protons at R_W=2.7 and 4.7 are significantly higher than those of the other AOT protons, while at R_W=0.2 they are nearly the same. This finding indicates that the pseudo-contact contribution to the ytterbium-induced shift of the nuclei in close proximity with the paramagnetic ion becomes more effective in the presence of water [33]. In other words, hydration of the surfactant head group could reduce the average ytterbium/H1, H1′ distance or could strengthen the dipolar interactions between Yb(III) and these protons.

SAXS spectra

Information on the size of salt-containing AOT reverse micelles were obtained by SAXS measurements of Yb $(NO_3)_3$, H_2O/AOT/n-heptane solutions at fixed AOT concentration ([AOT]=0.066 M) and two different R_W values (0.2 and 4.7) and various R_S ($0 \leq R_S \leq 0.1$). The experimental X-ray scattering patterns are shown in Fig. 12.

Because small-angle X-ray scattering arises from the contrast in electron density between different adjacent domains and considering the structure of reverse micelles, the scattering centers are to be considered the hydrophilic cores of AOT reverse micelles [7, 34, 35]. Taking into account that our samples can be considered dilute solutions of reverse micelles so that intermicellar interactions can be neglected and according to literature [36–38], all the SAXS spectra were analyzed by a model of non-interacting

Table 3 Chemical shifts (δ) of the water and AOT protons and *s* values (see text) of the $Yb(NO_3)_3$,H_2O/AOT/CCl_4 system

	δ (ppm)										
	R_S	R_W	CH_3		n-CH_2	H4,4′	H1′	H3′	H3	H1	H_2O
H_2O/AOT/CCl_4	0	0.2	0.54	0.56	0.94	1.21	2.77	3.58	3.73	3.94	3.09
$Yb(NO_3)_3$/AOT/CCl_4	0.01	0.2	0.57	0.60	0.97	1.24	2.81	3.62	3.77	3.98	2.15
	0.03		0.66	0.68	1.06	1.34	2.88	3.71	3.86	4.02	–
	0.05		0.81	0.83	1.21	1.48	3.05	3.86	4.01	4.21	–
	0.11		1.12		1.50	1.76	3.32	4.15	4.30	4.50	–
s			5.5		5.4	5.3	5.3	5.5	5.5	5.4	
H_2O/AOT/CCl_4	0	2.7	0.52	0.55	0.93	1.20	2.75	3.57	3.72	3.85	3.52
$Yb(NO_3)_3$/AOT/CCl_4	0.03	2.7	0.70	0.72	1.10	1.38	3.00	3.75	3.91	4.10	2.55
	0.05		0.81	0.83	1.21	1.49	3.15	3.86	4.04	4.24	1.81
s			5.6		5.5	5.7	7.9	5.7	6.3	7.7	
H_2O/AOT/CCl_4	0	4.7	0.52	0.55	0.92	1.20	2.74	3.57	3.72	3.81	3.70
$Yb(NO_3)_3$/AOT/CCl_4	0.03	4.7	0.70	0.72	1.10	1.37	2.95	3.75	3.90	4.04	3.21
	0.04		0.77	0.80	1.18	1.47	3.04	3.82	3.98	4.12	2.95
s			5.6		5.8	5.9	6.7	5.6	5.8	7.0	

polydisperse homogeneous scattering spheres. In particular, the smeared spectra $I(q)$ were fitted by the equation

$$I(q) \propto \int_0^\infty P(t) \int_0^\infty N(r) F^2(x) r^6 dr\, dt \tag{1}$$

where q is the elastic scattering vector and t is a variable defined along the length of the line-shaped primary X-ray beam with its intensity distribution function $P(t)$ [39]. $F(x)$ is the form factor of a sphere given by the equation

$$F(x) \propto \frac{\sin(x) - x\cos(x)}{x^3} \tag{2}$$

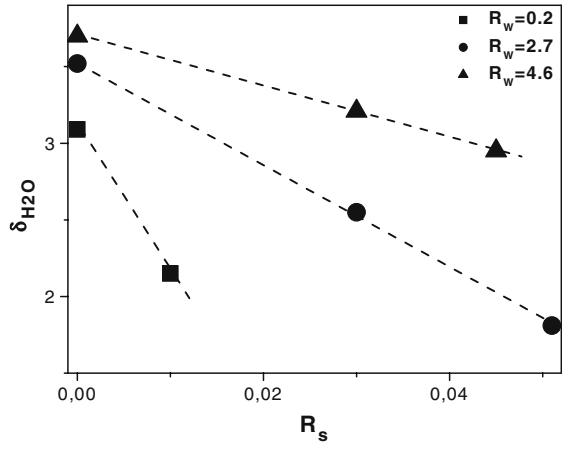

Fig. 10 Chemical shift of H_2O protons as function of R_S at various R_W values

where

$$x = r\sqrt{q^2 + t^2} \tag{3}$$

and r is its radius. $N(r)$, the size distribution function, is well-described by the Weibull equation [40]

$$N(r) = A\left(\frac{r}{r^\circ}\right)^{b-1} \exp\left[-\left(\frac{r}{r^\circ}\right)^b\right] \tag{4}$$

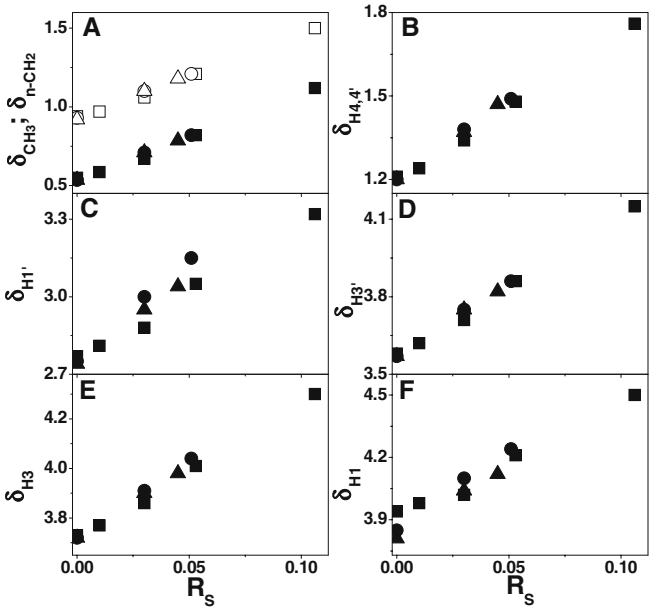

Fig. 11 Chemical shifts of AOT protons as function of R_S. **a** CH_2 protons at R_W=0.2 (□), R_W=2.7 (○), R_W=4.7 (△), and CH_3 protons at R_W=0.2 (■), R_W=2.7 (●), R_W=4.7 (▲). **b**–**f** R_W=0.2 (■), R_W=2.7 (●), R_W=4.7 (▲)

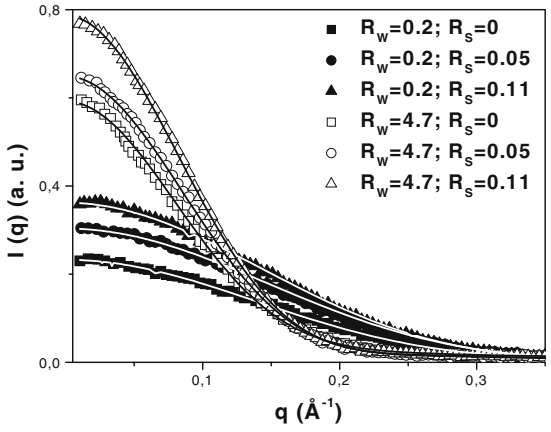

Fig. 12 SAXS patterns of $Yb(NO_3)_3$,H_2O/AOT/n-heptane system at various R_S and R_W

where A is a constant, b controls the shape of the size distribution function, and r° is related to the sphere mean radius r_m through the Γ function by

$$r_m = r^\circ \Gamma\left(\frac{b+1}{b}\right) \tag{5}$$

The continuous lines shown in Fig. 12 represent the fitting curves obtained by least-square analysis, and their agreement to the experimental points indicates that the SAXS spectra are adequately described by the employed model. The derived parameters, r_m and b, are collected in Table 4; while the corresponding size distribution functions of the core of AOT reverse micelles are shown in Fig. 13.

The mean radius of the bare micellar core at R_W=0.2 (r_m=10.7 Å) is in agreement with the literature value (r_m=9.4 Å) for bare AOT micelles in n-decane [36]. The value at R_W=4.7 (15.6 Å) compares favorably with those reported in the literature [37, 38, 41]. A perusal of Table 4 reveals that the micellar size and the size polydispersity increase significantly with the water content, while they remain practically independent on the R_S value. The effect of water addition on size and polydispersity has been widely discussed in the literature, and it will not be considered here [37, 38, 41]. It can be also noted that, at R_W=0.2, r_m and the polydispersity of reverse micelles are practically independent on the R_S value. This indicates that the structure of AOT reverse micelles is modestly impacted by the salt addition, i.e., the ytterbium salt is quite homogeneously distributed among the reverse micelles. In fact, considering a typical AOT aggregation number of about 20 and a homogeneous salt distribution, it can be calculated that only one or two salt molecules are entrapped in a reverse micelle. It is worth noting that this behavior is different from that observed when other salts, such as KBr, KCl, and $AgNO_3$, are entrapped in the AOT micellar core. In these cases, a marked increase of the size polydispersity is observed [8]. This indicates that, in general, the salt distribution among reverse micelles is system-specific, resulting from a delicate equilibrium between two opposite tendencies: unlimited growth and random dispersion among reverse micelles. Particularly in the case of Yb $(NO_3)_3$/AOT/organic solvent system, the second tendency prevails.

Table 4 Mean radius (r_m) and b values of the core of AOT reverse micelles ([AOT]=0.066 M) dispersed in n-heptane at various R_S and R_W

System	r_m (Å)	b
R_W=0.2; R_S=0	10.7±0.4	20±4
R_W=0.2; R_S=0.05	10.8±0.3	20±3
R_W=0.2; R_S=0.11	11.1±0.1	20±2
R_W=4.7; R_S=0	15.6±0.3	5.0±0.1
R_W=4.7; R_S=0.05	15.2±0.2	5.4±0.3
R_W=4.7; R_S=0.11	15.3±0.3	4.9±0.2

To acquire structural information on the $Yb(NO_3)_3$/AOT composites, SAXS measurements were also performed on some representative solid samples. The comparison between the SAXS spectra of $Yb(NO_3)_3$/AOT composites and pure AOT is shown in Fig. 14.

It is worth remembering that pure AOT possesses a two-dimensional hexagonal structure with long, mutually parallel AOT rods [42]. At first glance, the SAXS patterns of composites show two main features. The first is the absence of significant scattering in the range $0.01<q<0.2$ Å^{-1}, meaning that scattering objects dispersed in the surfactant matrix are absent in the composites, i.e., $Yb(NO_3)_3$ does not aggregate forming nanoparticles within the surfactant matrix. The second one is the presence of a peak at $q\approx0.3$ Å^{-1}, shifting at lower q by increasing R_S, which is due to the reflection of the 100 planes of the two-dimensional hexagonal array of the AOT rods [13]. The observed shift of the peak with R_S indicates an increase of

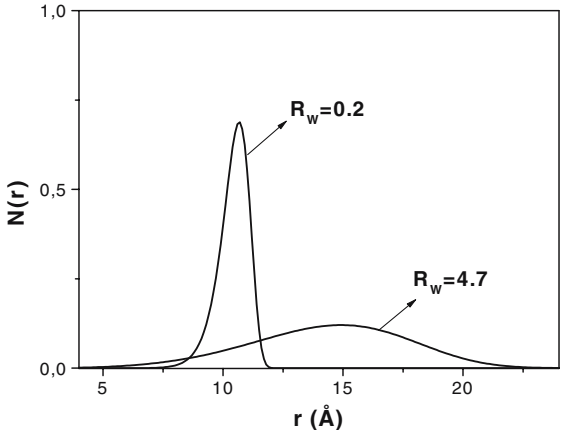

Fig. 13 Effect of water on the size distribution function of the core of AOT reverse micelles

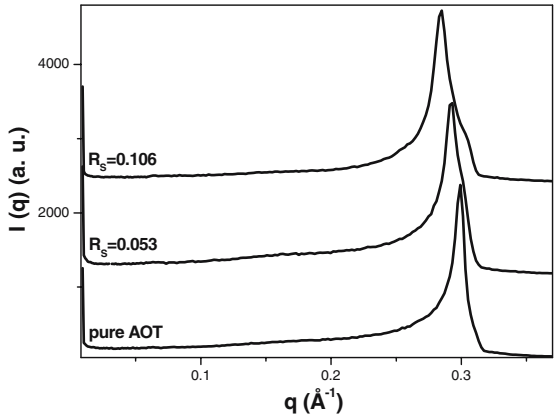

Fig. 14 Comparison between the SAXS spectra of pure AOT and $Yb(NO_3)_3$/AOT composites

the AOT 100 interplanar distance (d_{100}) attributable to the presence of the ytterbium salt entrapped in the hydrophilic core of AOT rods. To quantitatively evaluate this effect, the d_{100} were calculated from the q values at the peak maximum (q_{max}). These data are shown in Table 5. It is worth to note that d_{100} increases linearly with R_S and that this increase is quite modest, suggesting that $Yb(NO_3)_3$ is distributed in the hydrophilic domains of AOT liquid crystals as very small ionic clusters.

WAXS spectra

Further information on solid samples were achieved by wide-angle X-ray scattering (WAXS). WAXS spectra of some representative samples are shown in Fig. 15.

The absence in the $Yb(NO_3)_3$/AOT composite spectrum of peaks attributable to crystalline $Yb(NO_3)_3$ confirms that it is confined as very small and/or quite disordered entities. A broad reflection occurring at about 2θ=19.5° can be also observed due to the presence of an amorphous region constituted by the surfactant alkyl chains and two peaks occurring at about 4° and 8°, which can be attributed to the d_{100} and d_{200} interplanar distances, respectively [13]. From these peaks, interplanar distances in agreement with those found by SAXS were obtained.

Table 5 SAXS data of $Yb(NO_3)_3$/AOT composites at various R_S

System	q_{max} (Å^{-1})	d_{100} (Å^{-1})
Pure AOT	0.299	21.0
$Yb(NO_3)_3$/AOT R_S=0.05	0.292	21.5
$Yb(NO_3)_3$/AOT R_S=0.11	0.284	22.1

Conclusions

Through the synergic use of several techniques (solubility measurements, UV–vis–NIR, FT-IR, ^{1}H NMR, SAXS, and WAXS), it has been proven that $Yb(NO_3)_3$/AOT composites, containing very small-sized ionic clusters confined in the hydrophilic core of AOT reverse micelles, can be obtained by evaporation of volatile components (water and organic solvent) of $Yb(NO_3)_3$-containing w/o microemulsions. Salt confinement to form such clusters can be interpreted as possible, thanks to the water subtraction from salt-containing micellar aggregates in a sort of "confined crystallization" occurring during the evaporation process. It has been observed that such composites could be totally dispersed in n-heptane and CCl_4, allowing the solubilization of a relatively high amount of hydrophilic salt in a dry apolar medium. It has been also found that $Yb(NO_3)_3$/AOT/organic solvent resuspended composites are characterized by the presence of very small-size ionic clusters composed by Yb(III), NO_3^-, Na^+, and water traces surrounded by the anionic head groups of AOT and confined in the core of AOT reverse micelles. In reverse micelles at R_W=0.2, the ytterbium ions are mainly surrounded by nitrate anions and AOT SO_3^- groups, while by increasing R_W, these species are progressively substituted by water molecules. On the other hand, the spectral behavior of the nitrate ion at low R_w indicates that it is engaged in ion association, not only with the Yb(III) but also with the sodium counterion, in the confined space of the micellar core. Due to confinement effects and interaction with the hydrophilic species composing the micellar core, water appears to be translationally and rotationally restricted and strongly perturbed. Finally, the analysis of the SAXS and WAXS spectra of $Yb(NO_3)_3$/

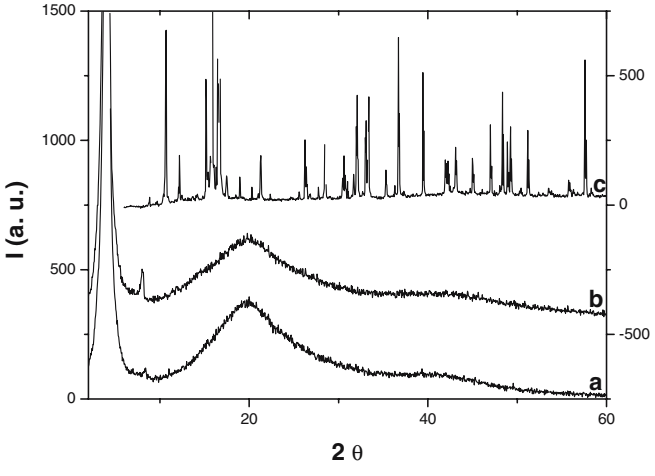

Fig. 15 Comparison between the X-ray powder diffraction patterns of pure AOT (**a**). $Yb(NO_3)_3$/AOT composite at R_s=0.11 (**b**). Pure solid $Yb(NO_3)_3 \cdot 5H_2O$ (**c**)

AOT composites indicates that, in such conditions, Yb $(NO_3)_3$ is dispersed in the surfactant matrix as very small ionic clusters confined in the hydrophilic domains of the typical hexagonal, bidimensional structure of AOT liquid crystals.

Acknowledgements Financial support from MIUR 60% and PRIN 2004 is gratefully acknowledged.

References

1. Turco Liveri V (1999) Curr Top Colloid Interface Sci 3:65
2. Marcianò V, Minore A, Turco Liveri V (2000) Colloid Polym Sci 278:250
3. Turco Liveri V (2001) Reversed micelles as nanometer-size solvent media. In: Rosoff M (ed) Nano-surface chemistry, vol. 1. Dekker, New York, pp 473–504
4. Giordano C, Longo A, Turco Liveri V, Venezia AM (2003) Colloid Polym Sci 281:229
5. Giordano C, Longo A, Ruggirello A, Turco Liveri V, Venezia AM (2004) Colloid Polym Sci 283:265
6. Calandra P, Longo A, Turco Liveri V (2001) Colloid Polym Sci 279:1112
7. Calandra P, Longo A, Turco Liveri V (2003) J Phys Chem 107:25
8. Calandra P, Longo A, Marcianò V, Turco Liveri V (2003) J Phys Chem 107:6724
9. Di Bari L, Pintacuda G, Salvatori P (2000) J Am Chem Soc 122:5557
10. Binnemans K, Gorlier-Walrand C (2002) Chem Rev 102:2303
11. Pileni MP, Zemb T, Petit C (1985) Chem Phys Lett 118:414
12. Rogers J, Winsor PA (1967) Nature (Lond) 216:477
13. Ekwall P, Mandell L, Fontell K (1970) J Colloid Interface Sci 33:215
14. Riter RE, Undekis EP, Kimmel JR, Levinger NE (1998) J Phys Chem 102:7931
15. Kitahara A, Kon-no K (1966) J Phys Chem 70:3394
16. Nitsch W, Plucinski P (1990) J Colloid Interface Sci 136:338
17. Onori G, Santucci A (1993) J Phys Chem 97:5430
18. Tomisic V, Simeon V (1999) Phys Chem Chem Phys 1:299
19. Eastoe J, Stebbing S, Dalton J, Heenan R (1996) Colloids Surf A Physicochem Eng Asp 119:123
20. Worley JD, Klotz IM (1966) J Chem Phys 45:2868
21. Giammona G, Goffredi F, Turco Liveri V, Vassallo G (1992) J Colloid Interface Sci 154:411
22. Li Q, Weng S, Wu J, Zhou N (1998) J Phys Chem B 102:3168
23. Calandra P, Caponetti E, Chillura Martino D, D'Angelo P, Minore A, Turco Liveri V (2000) J Mol Struct 522:165
24. Kanno H, Hiraishi J (1984) J Phys Chem 88:2787
25. Wahab A, Mahiuddin S (2004) J Chem Eng Data 49:126
26. Davis R, Irish DE (1968) Inorg Chem 7:1699
27. Ceraulo L, Dormond E, Mele A, Turco Liveri V (2003) Colloids Surf A Physicochem Eng Asp 218:255
28. Heatley F (1987) J Chem Soc Faraday Trans I 83:517
29. Bhattacharya PK, Lawson HJ, Barton JK (2003) Inorg Chem 42:8811
30. Heatley F (1988) J Chem Soc Faraday Trans I 84:343
31. Li Q, Li T, Wu J, Zhou N (2000) J Colloid Interface Sci 229:298
32. Novaki LP, Correa NM, Silber JJ, El Seoud OA (2000) Langmuir 16:5573
33. Cockerill AF, Davies GLO, Harden RC, Rackham DM (1973) Chem Rev 73:553
34. Mackeben S, Muller-Goymann CC (2000) Int J Pharm 196:207
35. North AN, Dore JC, McDonald JA, Robinson BH, Heenan RK, Howe AM (1986) Colloids Surf 19:21
36. Kotlarchyk M, Huang JS, Chen SH (1985) J Phys Chem 89:4382
37. Gochman-Hecht H, Bianco-Peled H (2005) J Colloid Interface Sci 288:230
38. Eastoe J, Fragneto G, Robinson BH, Towey TF, Heenan RK, Leng FJ (1992) J Chem Soc Faraday Trans 88:461
39. Ruland W (1974) J Appl Crystallogr 7:383
40. Aliotta F, Fontanella ME, Sacchi M, Vasi C, La Manna G, Turco Liveri V (1996) J Mol Struct 383:99
41. Hirai M, Kawai-Hirai R, Yabuki S, Takizawa T, Hirai T, Kobayashi K, Amemiya Y, Oya M (1995) J Phys Chem 99:6652
42. Ruggirello A, Turco Liveri V (2003) Chem Phys 288:187